

Spin-other-orbit interaction and magnetocrystalline anisotropy

M. D. Stiles,¹ S. V. Halilov,^{1,2} R. A. Hyman,³ and A. Zangwill²¹National Institute of Standards and Technology, Gaithersburg, Maryland 20899-8412²School of Physics, Georgia Institute of Technology, Atlanta, Georgia 30332-0430³Department of Physics, DePaul University, Chicago, Illinois 60614-3504

(Received 12 April 2001; published 23 August 2001)

We report the effect of the two-body, spin-other-orbit interaction on the magnetocrystalline anisotropy energy of the 3d transition metals. The relevant energy differences were computed for bcc Fe, fcc Ni, and hcp Co using a linearized augmented plane-wave method to solve the scalar relativistic Kohn-Sham equations in the local spin-density approximation. The spin-other-orbit interaction was incorporated at the level of the Hartree approximation. Special care was taken to guarantee the correctness of our numerical procedures. We find that the spin-other-orbit interaction does indeed change the anisotropy energy, but the effect is too small to account for the disagreement with experiment found in previous calculations for all three elements.

DOI: 10.1103/PhysRevB.64.104430

PACS number(s): 75.30.Gw, 71.15.Rf, 71.70.Ej

I. INTRODUCTION

The energy of a crystal ferromagnet is usually lowest when its magnetization points along a specific, high-symmetry, crystallographic direction. Nevertheless, the energy cost per atom to align the magnetization along some other direction can be remarkably small. For example, the measured *magnetocrystalline anisotropy* (MCA) energy $E_{MCA} = E(0001) - E(10\bar{1}0)$ is only $\approx 60 \mu\text{eV}$ per atom for hcp Co. The corresponding quantity for bcc Fe and fcc Ni is even smaller, $E_{MCA} = E(001) - E(111) \approx 1 \mu\text{eV}$ per atom.¹ The MCA is small² in these itinerant systems because the energy cost to reorient the magnetization is a relativistic effect. Indeed, the magnetization is aware of the lattice in bulk Fe, Ni, and Co only because the *spin-orbit interaction* couples the spin moment to the not-completely-quenched orbital moment at every atomic site in the crystal.³

The MCA energy is a ground-state quantity that falls within the purview of density-functional theory.⁴ In the Hartree approximation (see below), the theory actually involves *four* densities: the charge density, the current density, the magnetization density, and the polarization density. Nonetheless, current-density-functional calculations are still immature^{5,6} and we are unaware of any first-principles calculations of the electric polarization density in metals.⁷ Instead, most modern calculations⁸⁻¹³ of E_{MCA} use the local-spin-density approximation¹⁴ (LSDA) for the exchange and correlation parts of the energy functional.

The minuteness of the magnetocrystalline anisotropy energy presents special challenges to an LSDA electronic structure calculation. One issue is the accuracy of the method used to perform integrations over the occupied portion of the Brillouin zone. Another issue is precisely how the spin-orbit interaction is introduced. Most calculations use either the “force theorem”¹⁵ or a variational approach.⁸ For both, the spin orbit interaction is introduced at the end after a self-consistent calculation (without spin-orbit) has been performed. A third approach includes spin-orbit effects in a self-consistent manner.⁹

Figure 1 compares experimental data with results from

various high-quality LSDA calculations of E_{MCA} for the 3d transition metals. The best case is iron, where the computed values differ from experiment “only” by a factor of 2. The result for cobalt is far worse, and for nickel, the sign is not even correct. That is, the calculations predict the wrong easy axis. Nonetheless, with the exception of cobalt, we regard the clustering of the various results plotted in Fig. 1 as evidence that the computational issues can be brought under reasonable control.

It is difficult to escape the conclusion that some essential piece of physics is simply missing from the LSDA form of the exchange-correlation energy functional. One possibility is “orbital polarization” of the sort that leads to Hund’s second rule in atomic physics.¹⁶ An *ad hoc* procedure that models this phenomenon is known to improve orbital moment calculations.¹⁷ The same procedure applied to the present problem does indeed improve the calculated value of E_{MCA} for Fe, but not for Ni or Co.⁹ A related calculation¹⁸ exploits the so-called LDA+U method to account for intra-atomic correlation in an approximate manner. Good agreement be-

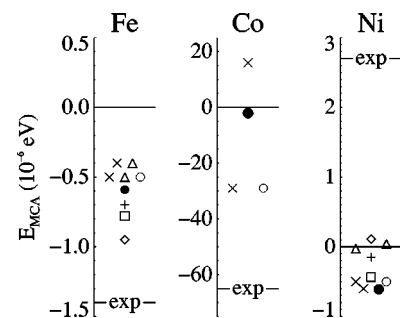


FIG. 1. Magnetocrystalline anisotropy for bcc Fe, hcp Co, and fcc Ni. The present results (●) are compared with experimental results (-exp-) from Ref. 1 and previous calculations, Ref. 8 (×), Ref. 9 (○), Ref. 10 (◇), Ref. 11 (△), Ref. 12 (□), and Ref. 13 (+). Where more than one of a symbol are given for a material, the two refer to *spd* and *spdf* basis sets in linearized-muffin-tin-orbital calculations. For Fe and Ni, $E_{MCA} = E(001) - E(111)$ and for Co $E_{MCA} = E(0001) - E(10\bar{1}0)$. For Co, $E(10\bar{1}0) = E(11\bar{2}0)$ in all converged calculations we have done.

tween theory and experiment for the anisotropy energy was reported with the choices $U=3.5$ eV for Fe and $U=4.0$ eV for Ni. However, the authors found $E_{\text{MCA}}(U)$ to be a very rapidly varying function for Ni (Ref. 18) and the theory predicts the wrong easy axis if $U=3.7$ eV as recommended by the most recent survey of a wide range of experiments.¹⁹

Given this state of affairs, it is not unreasonable to consider other effects that lie outside the LSDA. Accordingly, this paper reports electronic structure calculations of E_{MCA} for bcc Fe, fcc Ni, and hcp Co that include the so-called “spin-other-orbit” energy in the magnetic Hamiltonian. This contribution to the total energy is well known to emerge on an equal footing with the conventional “spin-same-orbit” energy when one goes beyond mean-field theory in a rigorous relativistic many-body theory of bound electrons.²⁰ A recent, formal, many-body study addressed to condensed matter problems examined the interplay between spin-same-orbit and spin-other-orbit effects at the level of the random-phase approximation.²¹

To our knowledge, the spin-other-orbit interaction has been neglected in all previous MCA studies. Presumably, this is so because early Hartree-Fock calculations²² attributed only about 10% of the spin-orbit parameter ξ to spin-other-orbit effects in the free $3d$ ions.²² We embarked on the study reported here nevertheless because the relevance of these calculations to LSDA wave functions in a hybridized solid was not obvious to us. As it turns out, they do indeed provide a good estimate (Fig. 1).

The remainder of this paper is organized as follows. Section II gives a simple classical argument to motivate the form of the spin-same-orbit and spin-other-orbit Hartree energy functionals and potentials used in our LSDA calculations. Section III describes the transformation of the formal theory into an efficient computational methodology and Sec. IV reports our results in detail. Section V is a summary and conclusion.

II. SPIN-ORBIT ENERGY AND MATRIX ELEMENTS

It is conventional to estimate spin-orbit effects in many-electron systems using the Hamiltonian²³

$$H_{\text{SO}} = \frac{1}{2m^2c^2} \sum_{i=1}^N \frac{1}{r_i} \frac{dV}{dr_i} \mathbf{L}_i \cdot \mathbf{S}_i. \quad (1)$$

This formula generalizes the spin-orbit term in the one-electron Pauli Hamiltonian (the nonrelativistic reduction of the one-electron Dirac equation) to a system of N noninteracting electrons that move in the central potential $V(r)$. Previous calculations of E_{MCA} for the $3d$ transition metals^{8–13} employ Eq. (1) using the self-consistently computed LSDA potential in an atomic sphere for $V(r)$. Spin-orbit effects in the interstitial volume are neglected and a spherically averaged form of H_{SO} may or may not be included in $V(r)$.

The argument for using the LSDA potential in H_{SO} is heuristic and has no formal justification. A more systematic approach begins with quantum-field theory and ends with a practical scheme to perform relativistic, many-body, elec-

tronic structure calculations for real systems.²⁰ To second order in the fine structure constant, it turns out that the self-consistent, mean-field Hamiltonian (including the usual scalar relativistic terms) should be supplemented by two-body terms of the sort first derived by Breit.²⁴ For present purposes, we need only the spin-orbit terms that emerge from the nonrelativistic reduction of the Breit energy.²⁵ The result for an N -electron system is

$$- \frac{e^2}{2m^2c^2} \frac{1}{4\pi\epsilon_0} \sum_{i=1}^N \sum_{j \neq i}^N \frac{(\mathbf{r}_i - \mathbf{r}_j) \times \mathbf{p}_i}{|\mathbf{r}_i - \mathbf{r}_j|^3} \cdot (\mathbf{S}_i + 2\mathbf{S}_j). \quad (2)$$

To gain some intuition, it is instructive to derive this expression semiclassically by writing down the spin-dependent energy terms that arise from the electric and magnetic interactions among the electrons:

$$U = - \sum_{i=1}^N \mathbf{m}_i \cdot \mathbf{B}(\mathbf{r}_i) - \sum_{i=1}^N \mathbf{d}_i \cdot \mathbf{E}(\mathbf{r}_i) + \sum_{i=1}^N \boldsymbol{\omega}_i \cdot \mathbf{S}_i. \quad (3)$$

The first term counts the potential energy of the magnetic dipole moment $\mathbf{m}_i = (q/m)\mathbf{S}_i$ of the i th electron in the magnetic field

$$\mathbf{B}(\mathbf{r}_i) = \frac{\mu_0}{4\pi} \sum_{j \neq i}^N q \mathbf{v}_j \times \frac{\mathbf{r}_i - \mathbf{r}_j}{|\mathbf{r}_i - \mathbf{r}_j|^3} \quad (4)$$

produced by all the other electrons.²⁶

The second term in Eq. (3) is the potential energy of the electric dipole moment $\mathbf{d}_i = -\mathbf{m}_i \times \mathbf{v}_i / c^2$ (acquired by a magnetic dipole that moves with velocity \mathbf{v}_i) in the electric field

$$\mathbf{E}(\mathbf{r}_i) = \frac{q}{4\pi\epsilon_0} \sum_{j \neq i}^N \frac{\mathbf{r}_i - \mathbf{r}_j}{|\mathbf{r}_i - \mathbf{r}_j|^3}, \quad (5)$$

produced by all the other electrons.²⁶ The last term is the electron-electron contribution to the change in rotational kinetic energy that occurs when the spin angular momentum of each electron precesses around the orbital center.²⁷ The precession is a relativistic effect that occurs because the electrons accelerate one another. Specifically,²⁸ if \mathbf{a}_i is the acceleration of the i th electron due to the other electrons, the electron-electron contribution to the precessional angular velocity is

$$\boldsymbol{\omega}_i = \frac{\mathbf{a}_i \times \mathbf{v}_i}{2c^2} = \frac{q\mathbf{E}(\mathbf{r}_i) \times \mathbf{v}_i}{2mc^2}, \quad (6)$$

when $v_i \ll c$.

With $q = -e$ and $\mathbf{p}_i = m\mathbf{v}_i$, it is easy to check that the electric dipole term and the Thomas precession term (exactly half as large as the dipole term but with the opposite sign) combine to give the usual spin-same-orbit term (proportional to \mathbf{S}_i) in Eq. (2). The less-familiar spin-other-orbit term (proportional to $2\mathbf{S}_j$) in Eq. (2) comes entirely from the magnetic dipole interaction.

Our interest is to incorporate the spin-same-orbit and spin-other-orbit interactions into the Hartree part of the Kohn-Sham energy functional. For this purpose, it is suffi-

cient to define reduced densities for charge, current, magnetic dipole moment (magnetization), and electric dipole moment (polarization) in terms of a set of two-component LSDA eigenfunctions $\psi_{i\sigma}(\mathbf{r})$ and their occupation numbers f_i :

$$\begin{aligned} n(\mathbf{r}) &= \sum_{i\sigma} f_i \psi_{i\sigma}^*(\mathbf{r}) \psi_{i\sigma}(\mathbf{r}) \\ \mathbf{j}(\mathbf{r}) &= -i \sum_{i\sigma} f_i \psi_{i\sigma}^*(\mathbf{r}) \nabla_{\mathbf{r}} \psi_{i\sigma}(\mathbf{r}) \\ \mathbf{m}(\mathbf{r}) &= \sum_{i\sigma\sigma'} f_i \psi_{i\sigma}^*(\mathbf{r}) \hat{\boldsymbol{\sigma}} \psi_{i\sigma'}(\mathbf{r}) \\ \mathbf{d}(\mathbf{r}) &= -i \sum_{i\sigma\sigma'} f_i \psi_{i\sigma}^*(\mathbf{r}) \hat{\boldsymbol{\sigma}} \times \nabla_{\mathbf{r}} \psi_{i\sigma'}(\mathbf{r}). \end{aligned} \quad (7)$$

In terms of these quantities, the Hartree energy function equivalent to Eq. (2) is written

$$\begin{aligned} H_{\text{SO}} &= \frac{\alpha^2 E_{\text{h}} a_0^3}{4} \int d^3 r \int d^3 r' \left\{ n(\mathbf{r}') \mathbf{d}(\mathbf{r}) \cdot \frac{\mathbf{r} - \mathbf{r}'}{|\mathbf{r} - \mathbf{r}'|^3} \right. \\ &\quad \left. - 2 \mathbf{j}(\mathbf{r}) \cdot \mathbf{m}(\mathbf{r}') \times \frac{\mathbf{r} - \mathbf{r}'}{|\mathbf{r} - \mathbf{r}'|^3} \right\}, \end{aligned} \quad (8)$$

where $\alpha = e^2/4\pi\epsilon_0\hbar c \approx 1/137.0$, $E_{\text{h}} = 4\pi\epsilon_0\hbar^2/me^2 \approx 27.21$ eV, and $a_0 = me^4/(4\pi\epsilon_0)^2\hbar^2 \approx 0.529$ nm.

The variational derivative of Eq. (8) with respect to $\psi_{i\sigma}(\mathbf{r})$ yields four terms—one from each density in Eq. (7)—that enter the Kohn-Sham equations. The corresponding matrix elements for basis functions $\chi_i(\mathbf{r})$ and $\chi_j(\mathbf{r})$ (with respective spin indices σ_i and σ_j) are

$$\begin{aligned} \langle \hat{H}_{\text{SO}} \rangle_{ji} &= \frac{\alpha^2 E_{\text{h}} a_0^3}{4} \int d^3 r \int d^3 r' \\ &\times \left\{ - \left[n(\mathbf{r}') \frac{\mathbf{r} - \mathbf{r}'}{|\mathbf{r} - \mathbf{r}'|^3} \right] \cdot [\chi_i^*(\mathbf{r}) \hat{\boldsymbol{\sigma}}_{\sigma_i\sigma_j} \times i \nabla_{\mathbf{r}} \chi_j(\mathbf{r})] \right. \\ &+ \left[\mathbf{d}(\mathbf{r}') \cdot \frac{\mathbf{r} - \mathbf{r}'}{|\mathbf{r} - \mathbf{r}'|^3} \right] [\chi_i^*(\mathbf{r}) \chi_j(\mathbf{r}) \delta_{\sigma_i\sigma_j}] \\ &+ 2 \left[\mathbf{m}(\mathbf{r}') \times \frac{\mathbf{r} - \mathbf{r}'}{|\mathbf{r} - \mathbf{r}'|^3} \right] \cdot [\chi_i^*(\mathbf{r}) i \nabla_{\mathbf{r}} \chi_j(\mathbf{r}) \delta_{\sigma_i\sigma_j}] \\ &\left. - 2 \left[\mathbf{j}(\mathbf{r}') \times \frac{\mathbf{r} - \mathbf{r}'}{|\mathbf{r} - \mathbf{r}'|^3} \right] \cdot [\chi_i^*(\mathbf{r}) \hat{\boldsymbol{\sigma}}_{\sigma_i\sigma_j} \chi_j(\mathbf{r})] \right\}. \end{aligned} \quad (9)$$

Of the four contributions to this matrix element, only the first spin-same-orbit piece appears in standard treatments of spin-orbit coupling. It is a single-particle-like term that cancels (in part) the spin-orbit coupling due to the nuclear potential. The second term in Eq. (9) is an alternate form of the first term that appears here because we have used an explicit two-body representation of the total energy. The fourth and third terms

are similarly equivalent contributions to the spin-other-orbit interaction. It is the effect of the last two on the MCA energy that is the main issue here.

III. METHOD OF CALCULATION

Collinear approximation. If the spins are described in a reference frame in which up and down are along $\hat{\mathbf{s}}$, the Pauli matrix can be written

$$\begin{aligned} \hat{\boldsymbol{\sigma}} &= \hat{\mathbf{s}}\sigma^z + \hat{\mathbf{u}}\sigma^x + \hat{\mathbf{v}}\sigma^y \\ &= \hat{\mathbf{s}}\sigma^z + \frac{1}{2} [(\hat{\mathbf{u}} + i\hat{\mathbf{v}})(\sigma^x - i\sigma^y) + (\hat{\mathbf{u}} - i\hat{\mathbf{v}})(\sigma^x + i\sigma^y)] \\ &= \left[\hat{\mathbf{s}} \begin{pmatrix} 1 & 0 \\ 0 & -1 \end{pmatrix} + (\hat{\mathbf{u}} + i\hat{\mathbf{v}}) \begin{pmatrix} 0 & 0 \\ 1 & 0 \end{pmatrix} + (\hat{\mathbf{u}} - i\hat{\mathbf{v}}) \begin{pmatrix} 0 & 1 \\ 0 & 0 \end{pmatrix} \right]. \end{aligned} \quad (10)$$

Here, the three directions

$$\hat{\mathbf{s}} = (\sin \theta \cos \phi, \sin \theta \sin \phi, \cos \theta) \quad (13)$$

$$\hat{\mathbf{u}} = (\cos \theta \cos \phi, \cos \theta \sin \phi, -\sin \theta) \quad (14)$$

$$\hat{\mathbf{v}} = (-\sin \phi, \cos \phi, 0), \quad (15)$$

make up an orthonormal set. In this representation, magnetization is

$$\begin{aligned} \mathbf{m}(\mathbf{r}) &= \hat{\mathbf{s}} [n_{\uparrow\uparrow}(\mathbf{r}) - n_{\downarrow\downarrow}(\mathbf{r})] + (\hat{\mathbf{u}} + i\hat{\mathbf{v}}) n_{\uparrow\downarrow}(\mathbf{r}) + (\hat{\mathbf{u}} - i\hat{\mathbf{v}}) n_{\downarrow\uparrow}(\mathbf{r}) \\ &\approx \hat{\mathbf{s}} \mathbf{m}(\mathbf{r}), \end{aligned} \quad (16)$$

where

$$n_{\sigma\sigma'}(\mathbf{r}) = \sum_{i'} f_{i'} \psi_{i'\sigma}^*(\mathbf{r}) \psi_{i'\sigma'}(\mathbf{r}). \quad (17)$$

The last step in Eq. (16) is the approximation that the spin density is collinear everywhere in space. This is rigorously true in the absence of spin-orbit coupling and spatially rotating magnetic fields. Spin-orbit coupling does generate noncollinear contributions, but these are small and have no rotationally invariant component around each atom. The noncollinear parts of the spin do not affect the energy significantly (in this problem) but they do greatly complicate the calculation of the exchange-correlation energy.

In the corresponding representation, the polarization is

$$\begin{aligned} \mathbf{d}(\mathbf{r}) &= \hat{\mathbf{s}} \times [\mathbf{j}_{\uparrow\uparrow}(\mathbf{r}) - \mathbf{j}_{\downarrow\downarrow}(\mathbf{r})] \\ &\quad + (\hat{\mathbf{u}} + i\hat{\mathbf{v}}) \times \mathbf{j}_{\downarrow\uparrow}(\mathbf{r}) + (\hat{\mathbf{u}} - i\hat{\mathbf{v}}) \times \mathbf{j}_{\uparrow\downarrow}(\mathbf{r}), \end{aligned} \quad (18)$$

where

$$\mathbf{j}_{\sigma\sigma'}(\mathbf{r}) = -i \sum_{i'} f_{i'} \psi_{i'\sigma}^*(\mathbf{r}) \nabla_{\mathbf{r}} \psi_{i'\sigma'}(\mathbf{r}). \quad (19)$$

It is worth noting that the polarization is smaller than the magnetization in absolute terms. However, unlike the mag-

netization, the parts of $\mathbf{d}(\mathbf{r})$, which are off-diagonal in the spin index, are comparable in magnitude to the diagonal parts and cannot be ignored. This is not a significant complication because the polarization does not enter the exchange-correlation energy in the local-spin-density approximation.

Spherical approximation. The dominant contributions to the spin-orbit interaction come from the spherical parts of the charge and spin densities. When the charge and spin densities are treated as spherical, $n(\mathbf{r}) \approx n(r)$ and $m(\mathbf{r}) \approx m(r)$, the gradient of the Coulomb interaction in the spin-orbit coupling energy can be replaced by

$$\begin{aligned} \frac{\mathbf{r}-\mathbf{r}'}{|\mathbf{r}-\mathbf{r}'|^3} &= -\nabla_{\mathbf{r}} \frac{1}{|\mathbf{r}-\mathbf{r}'|} \rightarrow 4\pi \frac{1}{r^2} \Theta(r-r') \hat{\mathbf{r}} Y_{00}(\Omega) Y_{00}^*(\Omega') \\ &= \frac{\hat{\mathbf{r}}}{r^2} \Theta(r-r'). \end{aligned} \quad (20)$$

With this replacement, the parts of the polarization and current that contribute to the energy (8) are

$$p(r) = - \int d\Omega \hat{\mathbf{r}} \cdot \mathbf{p}(\mathbf{r}) \quad (21)$$

$$j(r) = \int d\Omega \hat{\mathbf{s}} \cdot \hat{\mathbf{r}} \times \mathbf{j}(\mathbf{r}). \quad (22)$$

Integrating $rj(r)$ over r gives the orbital moment along $\hat{\mathbf{s}}$. In this approximation, the energy is

$$\begin{aligned} \langle \hat{H}_{\text{so}} \rangle_{\text{Har}} &= - \frac{\alpha^2 E_{\text{h}} a_0^3}{4} \left\{ 4\pi \int_0^\infty dr d(r) \int_0^r dr' r'^2 n(r') \right. \\ &\quad \left. + 8\pi \int_0^\infty dr j(r) \int_0^r dr' r'^2 m(r') \right\}. \end{aligned} \quad (23)$$

With atomiclike basis functions

$$\chi_i(\mathbf{r}) = \phi_i(r) Y_{l_i m_i}(\Omega), \quad (24)$$

the matrix elements (9) are

$$\begin{aligned} \langle \hat{H}_{\text{so}} \rangle_{ij} &= \frac{\alpha^2 E_{\text{h}} a_0^3}{4} \left\{ \int_0^\infty dr \phi_i(r) \phi_j(r) \frac{1}{r} \left[-4\pi \int_0^r dr' r'^2 n(r') \right] \left[\int d\Omega Y_{l_i m_i}^*(\Omega) \mathbf{L} Y_{l_j m_j}(\Omega) \right] \cdot \boldsymbol{\sigma}_{\sigma_i \sigma_j} \right. \\ &\quad + \int_0^\infty dr r^2 \phi_i(r) \phi_j(r) \left[- \int_r^\infty dr' d(r') \right] \delta_{l_i l_j} \delta_{m_i m_j} \delta_{\sigma_i \sigma_j} + 2 \int_0^\infty dr r^2 \phi_i(r) \phi_j(r) \left[- \int_r^\infty dr' j(r') \right] \delta_{l_i l_j} \delta_{m_i m_j} \sigma_{\sigma_i \sigma_j}^z \\ &\quad \left. + 2 \int_0^\infty dr \phi_i(r) \phi_j(r) \frac{1}{r} \left[-4\pi \int_0^r dr' r'^2 m(r') \right] \left[\int d\Omega Y_{l_i m_i}^*(\Omega) \mathbf{L} Y_{l_j m_j}(\Omega) \right] \cdot \hat{\mathbf{s}} \delta_{\sigma_i \sigma_j} \right\}. \end{aligned} \quad (25)$$

The first term is the coupling between the orbital angular momentum of an electron and its own spin. The fourth term is the coupling between the orbital angular momentum of an electron and the spins, assumed to be aligned along $\hat{\mathbf{s}}$, of the other electrons. The second term acts as a spin-independent potential and the third term acts like a spin potential.

LAPW approximation. We now incorporate these effects into a linearized-augmented-plane-wave (LAPW) electronic structure code²⁹ that solves the scalar relativistic Kohn-Sham equations in the local-spin-density approximation.³⁰ In the LAPW method, space is broken into spheres around each atom and the remaining interstitial region between atoms. In the calculations described here, the spheres are chosen to be as large as possible without overlapping. In the spheres, the charge, potential, and wave functions are described in an atomic-like manner in terms of radial functions times spherical harmonics, e.g., Eq. (24). In the interstitial, these quantities are described in terms of plane waves. While the full potential is used to describe the electrostatic and exchange-correlation potentials, we make the spherical approximation for the spin-orbit coupling. The spin-orbit coupling is small compared to these other energies and the non-spherical corrections are smaller still. Consistent with this approximation,

we ignore the spin-orbit interaction in the interstitial region. We use a frozen-core approximation so that we can compute anisotropies from the difference of valence energies on the order of 1000 eV instead of total energies on the order of 40 000 eV.

The magnetocrystalline anisotropy energy (MAE) is the difference in total energy when the magnetization points in two different high-symmetry directions. For hcp Co, we compute $E_{\text{MCA}} = E(0001) - E(10\bar{1}0)$. For bcc Fe and fcc Ni, we compute $E_{\text{MCA}} = E(001) - E(111)$. We compute the constituent energies in three different ways, discussed here in order of computational complexity. The first is based on the ‘‘force theorem,’’ discussed extensively by Daalderop *et al.*⁸ In this approach, a self-consistent calculation with no spin-orbit coupling is used to determine the input potential. Then the spin-orbit coupling is introduced and the eigenvalues are recomputed. The anisotropy is given by the difference in the eigenvalue sums for the different directions of the electrons’ spin. In this approach only the first and fourth terms in Eq. (25) play a role. When starting with a potential computed with no spin-orbit coupling, the second and third terms in Eq. (25) vanish because there is no current density or polarization in the input state.

TABLE I. Spin-orbit-coupling energy and magnetocrystalline anisotropy. Each column shows a different calculation of the spin-orbit coupling energy and the magnetocrystalline anisotropy, ft (force theorem), var (variational), and sc (self-consistent). All energies, given in μeV are relative to self-consistent results with no spin-orbit coupling. The first three columns of numbers are computed including spin-other-orbit coupling, and the last three columns are computed without it.

| | | | | | No spin-other-orbit coupling | | |
|----|------------------|------------------------|-------------------------|------------------------|------------------------------|-------------------------|------------------------|
| | | ΔE_{ft} | ΔE_{var} | ΔE_{sc} | ΔE_{ft} | ΔE_{var} | ΔE_{sc} |
| Fe | (001) | -5511.65 | -5511.79 | -6010.50 | -5466.72 | -5466.92 | -5963.11 |
| | (111) | -5511.17 | -5511.36 | -6009.91 | -5466.29 | -5466.54 | -5962.57 |
| | Diff. | -0.47 | -0.43 | -0.59 | -0.43 | -0.38 | -0.53 |
| Co | (0001) | -7066.75 | -7067.14 | -7809.75 | -6997.60 | -6998.07 | -7734.88 |
| | (10 $\bar{1}$ 0) | -7070.80 | -7071.31 | -7807.67 | -7004.54 | -7005.13 | -7736.04 |
| | Diff. | 4.05 | 4.17 | -2.07 | 6.93 | 7.06 | 1.16 |
| Ni | (001) | -8055.63 | -8056.19 | -8975.27 | -8034.93 | -8035.58 | -8952.55 |
| | (111) | -8055.10 | -8055.65 | -8974.66 | -8034.41 | -8035.05 | -8951.95 |
| | Diff. | -0.54 | -0.54 | -0.61 | -0.53 | -0.53 | -0.60 |

The second method extends the first approach by computing the total energy variationally using the same input potential as above. In this approach, both terms in Eq. (23) play a role in addition to the terms that contribute in the previous approximation. The anisotropy is given by the difference in the variational total energies. This approach requires storing not only the eigenvalues, but also the eigenvectors so that the densities can be computed once the Fermi level is determined.

Finally the third approach is to compute the energy fully self-consistently with the spin-orbit coupling included. In this case, the second and third terms in Eq. (25) play a role on the same footing as the other terms.

IV. RESULTS

Table I summarizes the results of a series of MAE calculations both with and without spin-other-orbit coupling. We see immediately that the differences between the force theorem calculations and the variational calculations are quite small. This is so because the initial calculation was done to a high degree of self-consistency. The energy difference increases by about 10% in magnitude when going to the fully self-consistent calculations.

Comparing the first three columns of Table I (spin-other-orbit present) with the last three columns of Table I (spin-other-orbit absent) shows that spin-other-orbit coupling makes at most a 10% change in the computed MAE relative to the experimental value. Indeed, the energy barely changes at all if we neglect the spin-same-orbit coupling and retain only the spin-other-orbit coupling. This is so because the (spin-other-orbit) $\mathbf{m} \cdot \mathbf{B}$ interaction in Eq. (3) is truly tiny unless the (spin-same-orbit) $\mathbf{p} \cdot \mathbf{E}$ coupling in Eq. (3) is *also* present to generate a non-negligible orbital current (and hence a non-negligible magnetic field) from the spin-polarized electron population. Unfortunately, the effect is not large enough to resolve the disagreement between calculation and experiment.

Our final results for the MAE are plotted as solid dots in

Fig. 1. Because the spin-other-orbit effect is small, they are in the same range as previous LSDA results,⁸⁻¹³ displayed in Fig. 1. Thus, the anisotropy for Fe has the same sign as the experimental results but is a factor of 2 too small. The MAE for Ni has the wrong sign and is about an order of magnitude too small. The Co prediction also agrees poorly with experiment. This is surprising because, according to conventional wisdom, the (relatively) large uniaxial anisotropy of this system should be more accurately computed with the LSDA than the smaller cubic anisotropies.

Evidently, it is important to establish that our calculations are numerically converged. Earlier calculations,⁸ based on the linearized-muffin-tin-orbital (LMTO) method, showed that the MAE for Co changed sign when the angular momentum cutoff for the wave functions increased from $l=2$ to $l=3$. Thus, it has *not* been established that LMTO calculations with even an $l=3$ angular momentum cut-off are numerically converged for this problem. We did not find such sensitivity in our LAPW calculations. These used angular momentum cutoffs of $l=6$ for the wave functions, charge, and potential in the atomic spheres and plane-wave cutoffs of $15 a_0^{-2}$ for the wave functions and $60 a_0^{-2}$ for the charge and potential in the interstitial region. While the total energy changes by much more than 10^{-6} eV when any of these parameters is varied around these values, the difference in energy between two different spin directions does not.

It is well known that the MAE is very sensitive to the convergence of integrations over the Brillouin zone in reciprocal space. We use the special k -points method³¹ where the integration is replaced by a sum over values on a discrete set of points in reciprocal space. These points are chosen to maintain the symmetry of the system by creating a set of points inside the Brillouin zone based on arbitrary sums of primitive reciprocal-lattice vectors that have been scaled down by some integer factor. For high-symmetry crystal structures like fcc and bcc, this scaling must be done with the same factor for each primitive reciprocal-lattice vector to maintain the symmetry. For structures with lower symmetry, like hcp, the scaling can be chosen differently for the out of

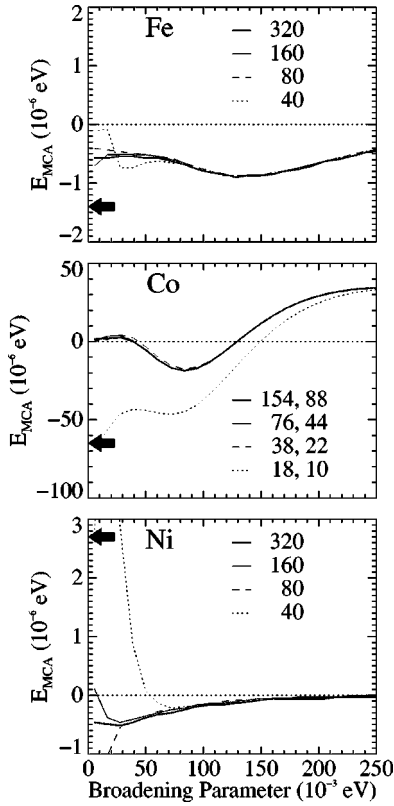


FIG. 2. Magnetocrystalline anisotropy for Fe, Ni, and hcp Co. The bottom, middle, and top panels, respectively, show the difference in energy between the (111) and (001) directions for Fe and Ni, and the (0001) and the (01 $\bar{1}$ 0) directions for Co. The curves give the calculated results as a function of the Fermi broadening parameter used in the k -space integration for different samplings of k space. An inset to each panel gives the number of divisions along each reciprocal lattice vector as described in the text. All results were computed from differences in the eigenvalue sums. The arrows close to the left axes indicate the zero-temperature experimental results.

plane direction than the in-plane directions in order to create a more-uniform sampling.

The special k -points method is poorly behaved for metallic systems unless it is augmented by some sort of smearing out of the Fermi level. For our work, we used a thermal broadening scheme where the occupancy of a state is given by the Fermi function with some fictitious temperature.³² Figure 2 illustrates our convergence tests for both k -point sampling and Fermi-surface smearing. The calculated MAE is plotted as a function of Fermi-surface smearing for a series of k -point samples. The different k -point samples are labeled by the inverse of the scaling factor for each of the primitive reciprocal-lattice vectors. For example, the curves for labeled 320 for Fe and Ni use uniform meshes of $320^3 = 32\,768\,000$ points in the full Brillouin zone. Symmetry reduces the number of these points that are independent. For spins pointed in the (111) direction, the irreducible wedge of the Brillouin zone is 12 times smaller than the full zone so that only 2 756 481 independent points were computed. As the scaling factor decreases by a factor of 2, the number of points in the full Brillouin zone decreases by a factor of 8.

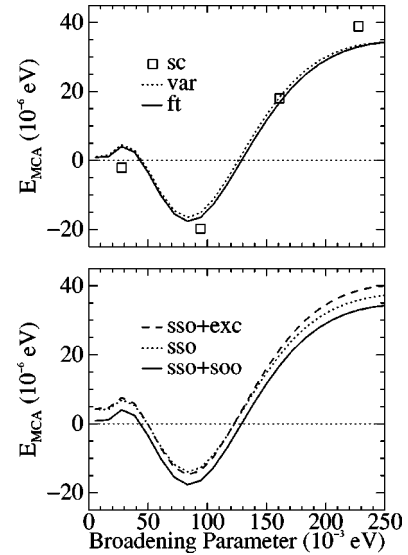


FIG. 3. Magnetocrystalline anisotropy for hcp Co. In both panels, the solid curve is the (38,22) curve from Fig. 2. The top panel compares calculations done comparing the force theorem (solid), the variational total energy (dotted), and the fully self-consistent total energy (symbols). The bottom panel compares calculations with (solid) and without (dotted and dashed) the contribution from spin-other-orbit coupling. The dashed curve includes the *ad hoc* contribution from the exchange-correlation potential as is typically used.

For Co, which is hcp, the scaling in the plane and out of the plane are independent. The first number associated with each curve is the scaling factor for the two in-plane primitive reciprocal-lattice vectors, and the second number is the scaling factor out of the plane. These pairs of numbers give k -point samples that are as close to uniform as possible.

In the calculations presented in Table I and those discussed below we use the $80 \times 80 \times 80$ k -point sample for Fe and Ni and the $38 \times 38 \times 20$ k -point sample for Co. These samples are not converged for Fermi-surface smearings smaller than about 30 meV, which is the value we use for the calculations presented in Table I. These convergence tests suggest that the temperature dependence is not important below this point. We would like to stress that in calculations in which the electronic structure is modified, convergence tests need to be redone.

Finally, Fig. 3 summarizes the effect of Fermi level broadening for various MAE calculations for cobalt. The top panel compares force theorem, variational, and self-consistent calculations. Similar calculations for Fe and Ni showed no difference between the three. The bottom panel shows the difference when the Hartree central potential in Eq. (1) does and does not include (as an *ad hoc* procedure) the LSDA exchange-correlation potential.

We conclude that the spin-other-orbit interaction makes a discernible, but not overwhelming contribution to the anisotropy. In particular, it is not enough to bring the LSDA-based calculations in agreement with experiment. In similar calculations for Fe and Ni, neither the exchange-correlation potential nor the spin-other-orbit coupling changed the calculated results beyond numerical precision.

V. CONCLUSION

In this work, we investigated the possibility that the heretofore neglected *spin-other-orbit interaction* might be responsible for the disagreement between the measured magnetocrystalline anisotropy energy of the 3d transition metals and previous theory. To this end, we incorporated the spin-other-orbit energy (in the Hartree approximation) into first-principles, LSDA calculations of the anisotropy energy for bcc Fe, fcc Ni, and hcp Co using the LAPW method. Taking care to ensure numerical convergence and accuracy with respect to Brillouin zone integrations, we found the effect of spin-other-orbit coupling to be far too small to bring previous LSDA theory and experiment in accord. The case of Co was particularly disappointing because the anisotropy energy in this uniaxial system is ten times larger than the MAE for Fe and Ni. No significant difference was found if the calculation was performed using the force theorem, variationally, or self-consistently.

It seems unlikely to us that the various technical approximations common to this sort of total-energy calculation

(frozen-core, spherical potentials in the atomic sphere, neglect of spin-orbit effects in the interstitial volume, scalar-relativistic plus spin-orbit central potential) are to blame for the disagreement between theory and experiment. The present work rules out the simplest sort of many-body effect. Earlier studies have implicated the approximate treatment of both exchange¹⁶ and correlation¹⁸ built into the LSDA exchange-correlation potential. We conclude that the issue remains unresolved and probably must await the development of a practical and justifiable extension of the local-spin-density approximation that can treat the angular momentum effects known to be important in atoms. Possibilities include current-density functional schemes, exact-exchange approaches, and generalizations of the orbital polarization approach.

ACKNOWLEDGMENTS

S.V.H. and A.Z. gratefully acknowledge the support of the National Science Foundation from NSF DMR-9531115.

-
- ¹M. B. Stearns, in *3d, 4d, and 5d Elements, Alloys and Compounds*, edited by H. P. J. Wijn, Landolt-Börnstein, New Series, Group III, Vol. 19, Pt. a (Springer, Berlin, 1986), p. 34.
- ²Of course, the bulk anisotropy is large because the exchange energy guarantees that all the spin moments act in concert.
- ³H. Brooks, Phys. Rev. **58**, 909 (1940); G.C. Fletcher, Proc. R. Soc. London, Ser. A **67**, 505 (1954).
- ⁴H.J.F. Jansen, Phys. Rev. B **38**, 8022 (1988); **59**, 4699 (1999).
- ⁵See, e.g., G. Vignale, in *Current Density Functional Theory and Orbital Magnetism*, edited by E. K. U. Gross and R. M. Dreizler (Plenum, New York, 1995), 485.
- ⁶H. Ebert, M. Bottonetti, and E.K.U. Gross, Europhys. Lett. **40**, 545 (1997).
- ⁷Of course, it is common to calculate the electric polarization in dielectrics where it arises from static charge displacements. See, e.g., R. Resta, Rev. Mod. Phys. **66**, 899 (1994).
- ⁸G.H.O. Daalderop, P.J. Kelly, and M.F.H. Schuurmans, Phys. Rev. B **41**, 11 919 (1990).
- ⁹J. Trygg, B. Johansson, O. Eriksson, and J.M. Wills, Phys. Rev. Lett. **75**, 2871 (1995).
- ¹⁰S.S.A. Razeef, J.B. Staunton, and F.J. Pinski, Phys. Rev. B **56**, 8082 (1997).
- ¹¹S.V. Halilov, A.Y. Perlov, P.M. Oppeneer, A.N. Yaresko, and V.N. Antonov, Phys. Rev. B **57**, 9557 (1998).
- ¹²S.V. Beiden, W.M. Temmerman, Z. Szotek, G.A. Gehring, G.M. Stocks, Y. Wang, D.M.C. Nicholson, W.A. Shelton, and H. Ebert, Phys. Rev. B **57**, 14 247 (1998).
- ¹³G. Schneider and H.J.F. Jansen, J. Appl. Phys. **87**, 5875 (2000).
- ¹⁴P. Hohenberg and W. Kohn, Phys. Rev. **136**, B864 (1964); W. Kohn and L.J. Sham, Phys. Rev. **140**, A1133 (1965); U. von Barth and L. Hedin, J. Phys. C **5**, 1629 (1972).
- ¹⁵M. Weinert, R.E. Watson, and J.W. Davenport, Phys. Rev. B **32**, 2115 (1985).
- ¹⁶H.J.F. Jansen, J. Appl. Phys. **67**, 4555 (1990).
- ¹⁷O. Eriksson, M.S.S. Brooks, and B. Johansson, Phys. Rev. B **41**, 9087 (1990).
- ¹⁸I. Yang, S.Y. Savrasov, and G. Kotliar, cond-mat/0006385 (unpublished).
- ¹⁹M.M. Steiner, R.C. Albers, and L.J. Sham, Phys. Rev. B **45**, 13 272 (1992).
- ²⁰J. Sucher, in *Relativistic Effects in Atoms, Molecules, and Solids*, edited by G. L. Malli (Plenum, New York, 1983), pp. 1–53.
- ²¹A.K. Rajagopal and M. Mochena, Phys. Rev. B **57**, 11 582 (1998).
- ²²M. Blume and R.E. Watson, Proc. R. Soc. London, Ser. A **271**, 565 (1963).
- ²³G. Baym, *Lectures on Quantum Mechanics* (Benjamin, Reading, MA, 1974).
- ²⁴G. Breit, Phys. Rev. **34**, 553 (1929); **36**, 383 (1930); **39**, 616 (1932).
- ²⁵H. A. Bethe and E. E. Salpeter, *Quantum Mechanics of One- and Two-Electron Atoms* (Plenum, New York, 1977), Sec. 39; V. B. Berestetskii, E. M. Lifshitz, and L. P. Pitaevskii, *Quantum Electrodynamics*, 2nd ed. (Pergamon, Oxford, 1980), Sec. 83.
- ²⁶J. C. Slater, *Quantum Theory of Atomic Structure* (McGraw-Hill, New York, 1960), Vol. II, Chap. 24.
- ²⁷This is the rotational analog of $\delta K = \delta(\frac{1}{2}mv^2) = m\mathbf{v} \cdot \delta\mathbf{v} = \mathbf{p} \cdot \delta\mathbf{v}$. See, e.g., G.P. Fisher, Am. J. Phys. **39**, 1528 (1971).
- ²⁸L.H. Thomas, Philos. Mag. **3**, 1 (1927).
- ²⁹L.F. Mattheiss and D.R. Hamann, Phys. Rev. B **33**, 823 (1986).
- ³⁰J.P. Perdew and Y. Wang, Phys. Rev. B **45**, 13 244 (1992).
- ³¹H.J. Monkhorst and J.D. Pack, Phys. Rev. B **13**, 5188 (1976).
- ³²For an extensive discussion of various schemes for Brillouin zone integration and Fermi surface smearing, see G. Schneider and H. J. F. Jansen (unpublished), Web site <http://www.physics.orst.edu/~henri/Jansen.html>.